2D balance control of a self-balancing robot for power inspection in urban networks

[iD] Vinícius Moreno Sanches [1]*

[iD] Pedro Bortolon Pereira da Cunha [2]

[iD] Henrique Simas [3]

[iD] Julio Elias Normey-Rico [4]

[iD] Marco Antonio Martins Cavaco [5]

[1] viniciuseislaine@gmail.com
[2] pedro.b.p.cunha@gmail.com
[3] henrique.simas@ufsc.br
[4] julio.normey@ufsc.br
[5] cavaco@labmetro.ufsc.br

Universidade Federal de Santa Catarina (UFSC), Brazil

*Corresponding author.

ABSTRACT: The power inspection of energy transmission networks is an effective way of mitigating risks, and failures, and avoiding mistakes in the transmission system. However, the inspection market is highly competitive and has difficulties in this process, mainly due to the high altitude of the lines. A standard solution for inspection of high-altitude power lines can be implemented using drones and aircraft, however, has a high cost for operation and poor logistics viability. In this scenario, "Prof. Raul Guenther's Robotic Lab" developed a project of a robot that goes through low and medium-voltage wires to power inspection of transmission systems in urban networks. In this paper we propose the use of a self-balancing robot, aiming to execute the inspection, using a 2D balance control to stabilize the balance on the cable. Moreover, we evaluate the viability and effectiveness of the proposed control strategy, highlighting its advantages and properties using numerical simulations considering a non-linear model, and expected disturbances. Moreover, we develop computational experiments with graphical results, simulating the model in different situations to find the limits of the controller, based on the maximum speed of the wind and the robot moving through the wires.

Keywords: electric power transmission; power inspection; self-balancing robot; urban electric networks.

Controle de equilíbrio 2D de um robô autoequilibrado para inspeção de energia em redes urbanas

RESUMO: *A inspeção de redes de transmissão de energia é uma maneira efetiva de mitigar riscos, falhas e evitar erros na operação do sistema de transmissão de energia. Entretanto, o mercado de inspeção é altamente competitivo e possui diversas dificuldades nesse processo, principalmente devido à alta altitude das linhas. Uma solução padrão para a inspeção dessas linhas de energia em alta altitude consiste no uso de drones e helicópteros, que possuem um alto custo para operação e baixa viabilidade logística. Nesse cenário, o Laboratório*

de Robótica Prof. Raul Guenther está desenvolvendo um projeto de um robô que percorre linhas de baixa e média tensão para sistemas de transmissão de energia em redes urbanas. Neste artigo propomos o uso de um "robô autoequilibrado" visando à execução dessa inspeção, projetando um controle de equilíbrio 2D para esse robô. Além disso, avalia-se a viabilidade e eficácia desse controlador proposto, destacando-se suas vantagens e propriedades usando simulações numéricas para um modelo não linear, adicionando sinais de perturbação. Para validação da proposição, experimentos computacionais foram desenvolvidos com resultados gráficos, simulando o modelo em situações diferentes a fim de encontrar os limites do controlador, com base na velocidade máxima de vento e na movimentação do robô pelos fios.

Palavras-chave: inspeção de energia; redes elétricas urbanas; robô autoequilibrado; sistemas de transmissão de energia.

1 Introduction

From the process of urbanization in Brazil, between 1950 and 1980 (Santos, 2013), electricity has become a vital resource not only for industries and companies but also in people's daily lives as presented in the paper of Barbosa and Veloso (2014).

Today, approximately 68.1% of electric power in Brazil is generated from hydroelectric plants, due to the water potential of the country (Oliveira, 2018). This brings an important advantage because that is a fundamental renewable energy source for the sustainability of natural resources (Kaygusuz, 2002). However, these hydroelectric plants are located mostly in rural areas, far from the urban area. In that case, it is necessary to have a power transmission tower infrastructure (Doukas *et al.*, 2011), responsible for carrying that energy to the civilization. In this context, the urban networks appear as a great point of interest for our studies.

Such power transmission systems are the study object of the scientific community, as presented in the papers of Adabo (2014), Han, Hao and Lee (2009), and Luque-Vega *et al.* (2014). This happens because of the competitiveness factor that these systems bring to the energy companies, mainly in the scope of inspections and preventive and predictive maintenance (Zhang *et al.*, 2009).

With the current technology in Brazil, power line inspection is made mainly using manned helicopters (Xie *et al.*, 2017). But because of the high cost, high dangerousness, and low viability, it urges interest in the study of new solutions, looking for cheaper and more viable options for the process of inspection in power transmission systems.

In this context, "Prof. Raul Guenther Robotic Lab" from Universidade Federal de Santa Catarina (UFSC) developed research aiming to project a self-balancing robot that goes through low and medium-voltage wires for inspection in power transmission systems in urban networks. Similar research can be found in the papers of Alhassan *et al.* (2020), Jalal *et al.* (2018), Roussialian *et al.* (2019), and Shaikat, Hussein and Tasnim (2021).

Such papers find, amongst others, some main issues regarding the battery limit of robots and wind disturbances, concluding that these factors should be considered in future research.

Therefore, the objective of this paper is to propose theoretically, through numerical simulations, a 2D balance control of a mobile robot for displacement and inspection of

urban networks. Moreover, a study regarding the physical limits of the proposed controller is presented, as well as some mechanical approaches that can be aimed at the balancing robot. This paper contributes with an analysis of control strategies for self-balancing robots, looking for battery limits and wind disturbances. In addition, this work is based on numerical simulations.

The paper is organized as follows. Section 2 describes the proposed self-balancing robot and its controller, considering reaction wheel-balanced inverted pendulum equations. Section 3 brings the experimental results and new proposals for controllers over these results. Section 4 compiles the final results and discussions. Then, section 5 concludes the paper.

2 Research method and scope

This paper deals with the numerical environment modeling and simulation of robot dynamics based on a CAD model at the prototype level. The dynamic model used is based on equations presented in other scientific works (Belascuen; Aguilar, 2018), associating the study of performance, complexity, and feasibility of several control strategies.

2.1 Proposed self-balancing robot

The robot used for the studies is a self-balancing robot with two reaction wheels for balance control (frontal and lateral), as illustrated in Figure 1.

Figure 1 ▶
Illustration
of a proposed
self-balancing robot.
*Source: elaborated by
the authors*
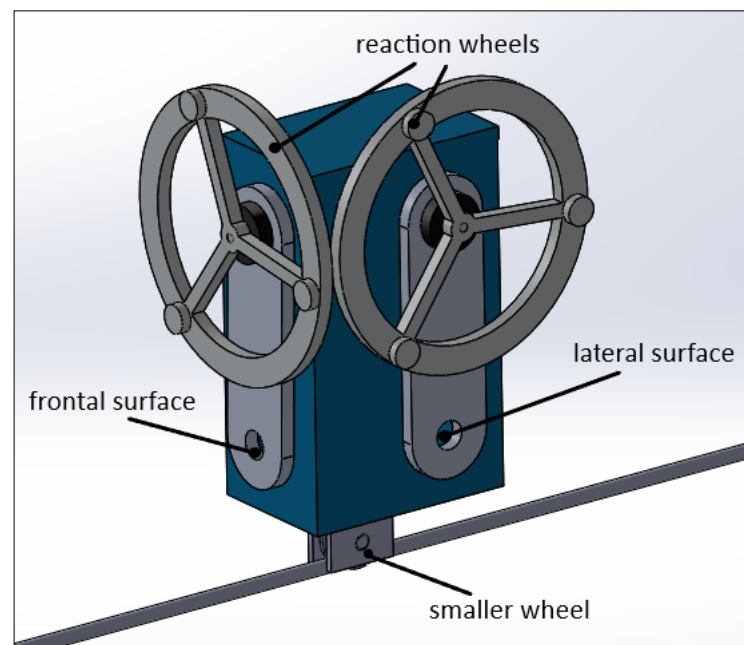
The robot design, as well as all sensor compartments, was simplified as a blue box with a mass identical to the robot. Attached to the robot we have two reaction wheels: the first on the frontal surface, and a second on the lateral surface.

A smaller travel wheel establishes a fitting connection between the robot and the wire, allowing its displacement.

Subsection 2.2 presents the modeling of the system based on a classic case of a reaction wheel balanced inverted pendulum, due to the similarity between the systems (Belascuen; Aguilar, 2018).
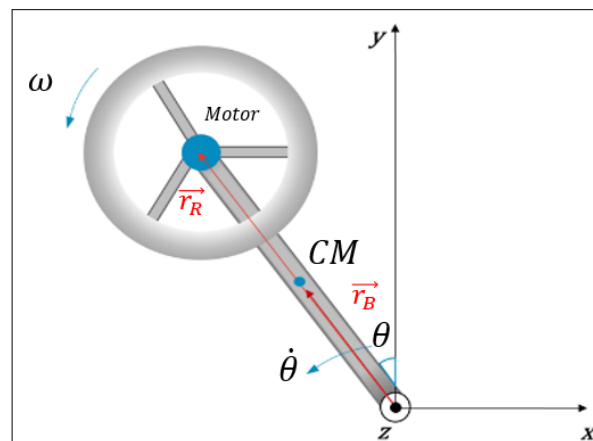
2.2 Dynamic reaction wheel balanced inverted pendulum model

To implement an effective control system, with physical and mathematical fundamentals, it is necessary to understand the model of the system that we are working on, starting from equations that describe mainly the behavior of the pendulum angle (θ), and its relation to other variables as, for example, the motor voltage ($u(t)$). To model this system, we rely on the work of Belascuen and Aguilar (2018).

2.2.1 Non-linear model (lateral balance)

Figure 2 presents the self-balancing robot in frontal view with its respective base frame and the following parameters:

- $\vec{r}_B, \vec{r}_R$: position vector of the center of mass of the arm, and the wheel mass respectively, that coincides with the position vector of the motor;
- M_M, M_R, and M_B: mass of the motor, mass of the wheel, and the mass of the robot body, respectively;
- g: acceleration of gravity;
- I_M, I_B, I_R, and I_{CM}: moment of inertia of the motor, the body, wheel, and moment of inertia of the wheel with respect to your center of mass, respectively;
- τ_{at} and τ_M: resultant torque from friction and mechanical torque of the motor, respectively;
- ω, $\dot{\omega}$ and ω_z: angular velocity and acceleration of the wheel measured by a fixed observer and with a reference frame fixed to the wheel, respectively;
- τ_e, k, R and i: electrical torque, constant characteristic, resistance, and electrical current of the motor, respectively.
- $\theta, \dot{\theta}, \ddot{\theta}$: general angular position, velocity, and acceleration, respectively.

Firstly, by Newton's second law to the rotation, we have $\sum \vec{\tau} = I \cdot \ddot{\vec{\theta}}$. Once all torques have the same direction, we can adopt a scalar treatment, considering the hypothesis that: $\vec{\tau} = \vec{r} \times \vec{F}$, where $\vec{r}$ is a general distance vector of torque, and $\vec{F}$ is a general force applied. If we consider the point of origin as the pole rotation, we have Equation 1.

$$M_M g r_R \sin(\theta) + M_B g r_B \sin(\theta) + M_R g r_R \sin(\theta) - \tau_{at} - \tau_M = (I_M + I_B + I_R)\ddot{\theta} \quad (1)$$

Analyzing the rotation movement of the wheel, we can write, using the fixed reference frame:

$$\tau_M = \dot{\omega} I_{CM} = \tau_e - \tau_{at} \quad (2)$$

The electrical torque is assumed as proportional to the electrical current (I), with $\tau_e = k_1 I$, where k_1 is the electrical constant of the torque. Now, in Equation 2, we can change the reference frame from Earth to the wheels as follows:

$$\omega = \omega_z + \dot{\theta} \quad (3)$$

Eventually, the last equation relates the voltage measured in motor terminals (U), we consider the voltage caused by the self-inductance, as we assume the electrical current as constant, where k_2 is another electrical constant of the voltage:

$$U - k_2 \omega_z = R \times i \quad (4)$$

2.2.2 System disturbances (lateral balance)

The main disturbance of the system, for lateral balance, is the wind speed affecting the robot. To model this impact, we rely on the work of Du *et al.* (2009), considering a linear speed, applied at a central point in the lateral surface of the robot. The authors describe the torque by the equation:

$$\tau_q = F_{wind} r_m = C_a 0.613 q(t)^2 A_e r_m \quad (5)$$

where: $q(t)$: wind speed in m/s; r_m : distance from the center of mass of the robot to the wire; C_a: surface drag coefficient; A_e: area of wind incidence; and F_{wind}: force of wind.

With this, the Equation 1 becomes:

$$M_M g r_R \sin(\theta) + M_B g r_B \sin(\theta) + M_R g r_R \sin(\theta) - \tau_{at} - \tau_M - \tau_q = (I_M + I_B + I_R)\ddot{\theta} \quad (6)$$

2.2.3 Friction torque

The proposed model has unknown variables: torque and friction forces. So, in this case, to simplify the system, we will adopt a model (Olsson $et\ al.$, 1998) where the friction is given by $\tau_{at} = b \cdot w_z$, that is, it increases proportionally to the relative speed between the contact surfaces. The constant depends on the materials used.

2.2.4 The dynamic linear model and its representation of the model in state-space equations

To simplify the modeling of the problem, we can consider that the controller can keep the system around the point of equilibrium given by $\theta \approx 0$ rad. With this hypothesis, Equation 6 turns into:

$$M_M g r_R \theta + M_B g r_B \theta + M_R g r_R \theta - \tau_{at} - \tau_M - \tau_q = (I_M + I_B + I_R) \ddot{\theta} \qquad (7)$$

Thus, defining the state-space variables (Belascuen; Aguilar, 2018):

- $x_1 = \theta$ (angular position, given in rad);
- $x_2 = \dot{\theta}$ (angular speed, given in $\frac{rad}{s}$);
- $x_3 = \omega_z$ (reaction wheel angular speed, given in $\frac{rad}{s}$).

Employing this definition, we obtain the state-space equations for the lateral balance of the robot:

$$\dot{x}_1 = x_2 \qquad (8)$$

$$\dot{x}_2 = \frac{Kmgl}{Iso} x_1 - \frac{Bb}{Iso} x_2 + \frac{\left(\dfrac{KtKe}{R} + Br\right)}{Iso} x_3 - \frac{Kt}{RIso} U(t) + \frac{2 C_a 0{,}613 A_e r_m}{Iso} q(t) \qquad (9)$$

$$\dot{x}_3 = \frac{-Kmgl}{Iso} x_1 + \frac{Bb}{Iso} x_2 - \frac{Iso + I_R}{Iso\,I_R}\left(Br + \frac{KeKt}{R}\right) x_3 + \frac{Iso + I_R}{Iso\,I_R}\left(\frac{Kt}{R}\right) U(t) \qquad (10)$$

where $K_{mgl} = (M_M r_R + M_b r_b + M_R r_R) g$ and $Iso = (I_M + I_b + I_R)$.

From the Equations 8, 9, and 10 we can represent a state-space system in the following way:

$$\begin{cases} \dot{X} = AX + Bu(t) \\ y = CX + Du(t) \end{cases} \qquad (11)$$

where $\dot{X} = [\dot{x}_1, \dot{x}_2, \dot{x}_3]^T$, y is the process variable, and A, B, C, and D are:

$$A = \begin{bmatrix} 0 & 1 & 0 \\ \dfrac{Kmgl}{Iso} & \dfrac{-Bb}{Iso} & \dfrac{\left(\dfrac{KtKe}{R} + Br\right)}{Iso} \\ \dfrac{-Kmgl}{Iso} & \dfrac{Bb}{Iso} & \dfrac{-Iso + I_R}{Iso\, I_R}\left(Br + \dfrac{KeKt}{R}\right) \end{bmatrix} \tag{12}$$

$$B = \begin{bmatrix} 0 & 0 \\ \dfrac{-Kt}{R \cdot Iso} & \dfrac{2\,C_a\,0{,}613\,A_e\,r_m}{Iso} \\ \dfrac{Iso + I_R}{Iso\, I_R}\left(\dfrac{Kt}{R}\right) & 0 \end{bmatrix} \tag{13}$$

$$C = \begin{bmatrix} 1 & 0 & 0 \end{bmatrix} \tag{14}$$

$$D = \begin{bmatrix} 0 \end{bmatrix} \tag{15}$$

2.2.5 System parameters

For testing and simulation purposes, it was required to define theoretical parameters for our system (lateral balance). These parameters were based on some existing components such as the 770 series Transmotec™ motors (Transmotec, 2021), as presented in Table 1.

Table 1 ▶
Parameters used in
simulations (lateral balance).
Source: experimental data

Symbol	Parameter	Value
Bb	Friction coefficient (*rad/s*)	0.492
Mb	Arm mass (*kg*)	0.15624
Mr	Robot mass (*kg*)	0.1
Mm	Motor mass (*kg*)	0.05
r_b	Distance from the center of the mass of the arm to the rotation axle (*m*)	0.09
r_m	Distance from the center of the mass of the motor to the rotation axle (*m*)	0.195
r_R	Distance from the center of the mass of the robot to the rotation axle (*m*)	0.195
kt	Motor torque constant	0.0663
ke	Motor electrical constant	0.0663
R	Motor resistance (*mΩ*)	2.7289
L	Motor inductance (*mH*)	2.473
Br	Friction coefficient of the motor	0.000138
Ca	Drag coefficient of the robot	1.4
Ae	Incidence area of the wind (m²)	0.12

2.3 Proposal for a lateral balance controller

From the model found in Equation 11, we can propose a simple and feasible control strategy state observation feedback controller (Ogata, 2010).

Once the system is completely observable, it is possible to project a state observer that, by the sensing of just one state variable, can estimate the other two. Combining that with a controller, we can control the system as required.

Choosing the damping and response-time of the control closed-loop as $\xi = 0.5$ and $t_{5\%} = 1.5\ s$ respectively, the desired closed-loop control poles were adjusted as:

$$s=-2+2\sqrt{3}\,j\,,s=-2-2\sqrt{3}\,j\,,s=-6 \tag{16}$$

and the poles are chosen to the observer located as in Equation (17):

$$s=-20\,,s=-20 \tag{17}$$

Thus, using the codes proposed in Ogata (2010), we obtain the state feedback array K and the gain array K_e of the observer in:

$$K=\begin{bmatrix}-0.9249 & -0.9249 & -0.9249\end{bmatrix}$$

$$K_e=\begin{bmatrix}-27.2835 \\ 535.4301\end{bmatrix} \tag{18}$$

Eventually, with the feedback array defined, we can find the transfer function of the controller, given in Equation (19):

$$C(s)=\frac{-56.6125\,s^2+1.7\cdot10^3\,s-1.04\cdot10^3}{s^2-17.28\,s+830.76} \tag{19}$$

## 3 Experimental results and adjustments to the controller

To test this controller theoretically, we simulate a scenario considering the robot as a linear system and with an initial condition of $\theta = 0.1$ rad. Also, it was considered a battery with a limit of a 24 V voltage, and this physical limit was represented as a saturation block in the Simulink™ environment. The block diagram of this simulation is illustrated in Figure 3.

Figure 3 ▼
Block diagram used for the simulations. Linear case model without disturbances.
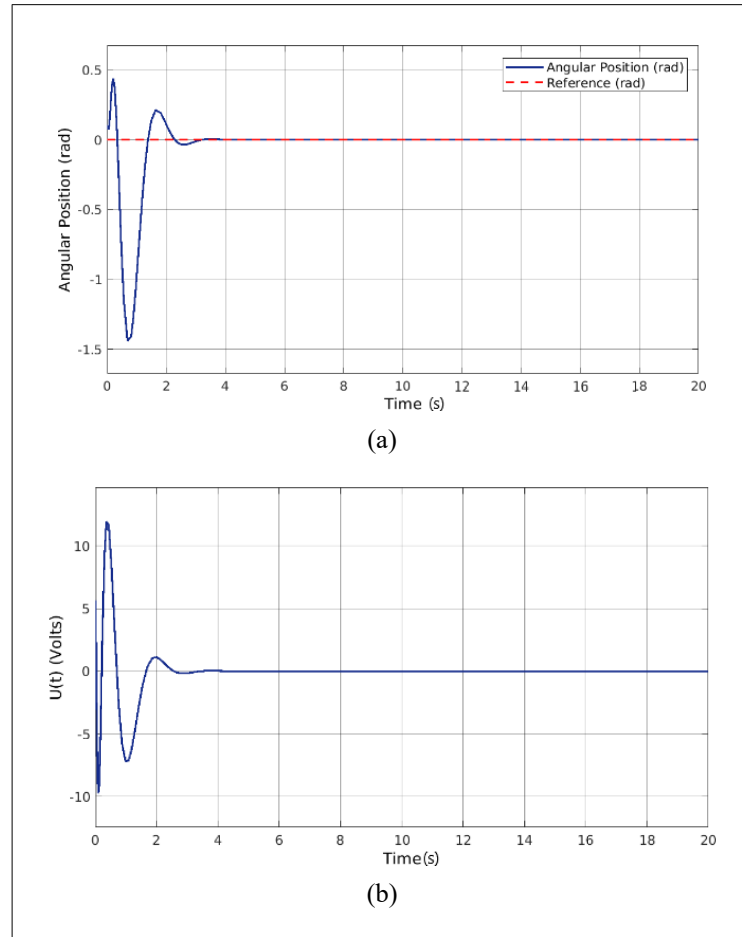*Source: experimental data*
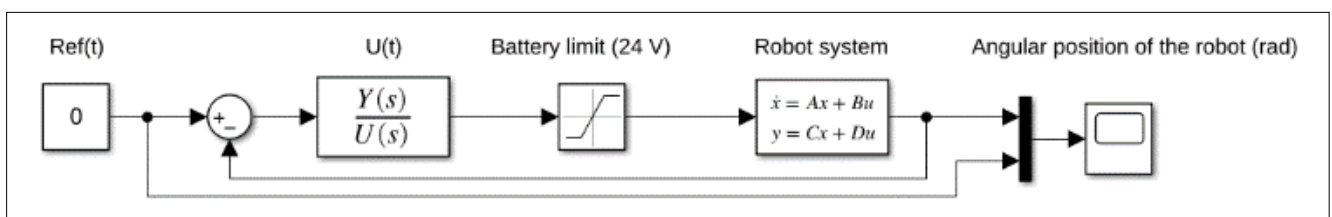
3.1 Control analysis

By using the projected control strategy in Equation (19), we can observe, by the graphic result presented in Figure 4, that the project takes the angular position to the reference effectively, with the control variable respecting the physical limits of the battery.
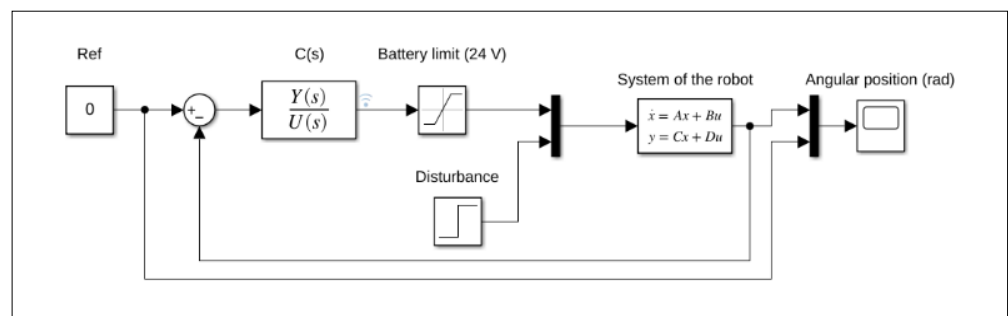
(a)

(b)

The proposed controller has good performance in the linear system without disturbances, as it is expected. Moreover, it is necessary to test it in more complex systems, so we will apply disturbances of wind $q(t)$ and analyze the results, as well as the viability, i.e., the control action must be under the limit of 24 V of battery.

Therefore, to simulate the system with disturbances it was used a block diagram of Figure 5 was used relying on the equations from subsection 2.2.4.
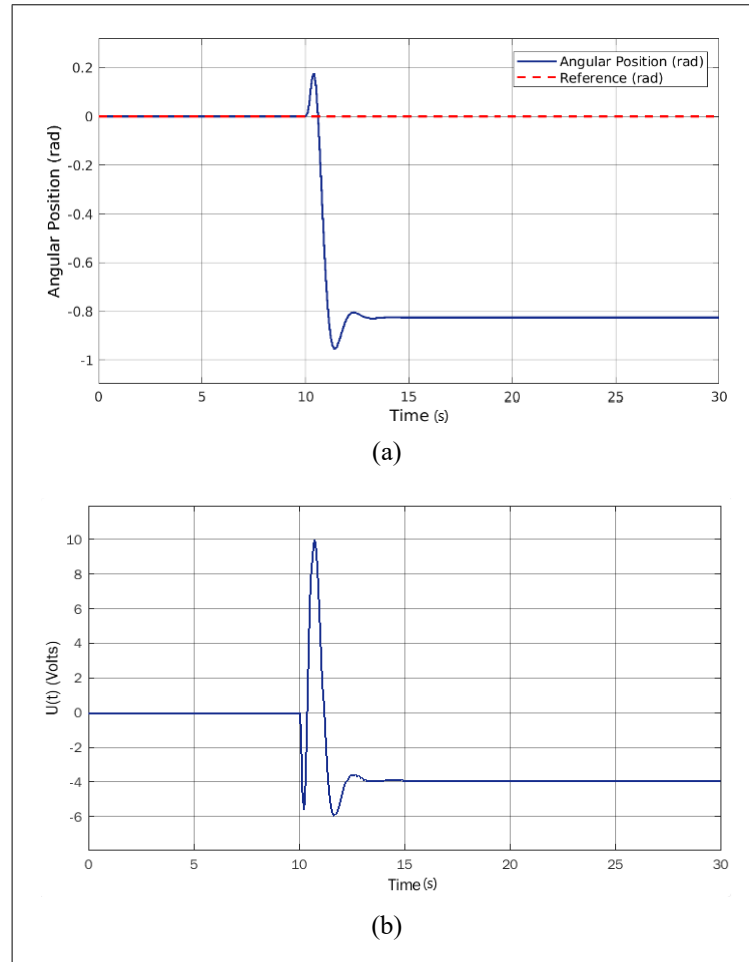
In this simulation, it was considered a wind affecting the lateral surface of the robot with a hypothetical speed of 2 m/s (approximately 3.89 knots) for the first 10 s of the simulation. The obtained graphic result is given in Figure 6. Note that the controller guarantees the stability of the system but fails to eliminate the steady-state error.

(a)

(b)

To eliminate the steady-state error, we propose a controller, by adding an integrator to the state observation feedback control law previously proposed. Using similar steps as in section 2.3 we obtain a new feedback controller, shown in Equation (20).

$$C(s)=\frac{-6.6\,s^3+3.9\cdot10^3\,s^2-2.2\cdot10^3\,s+0.5}{s^3-0.3\,s^2+1.8\cdot10^3\,s} \qquad (20)$$

To test this controller, we simulate it in the proposed non-linear model, which has a more realistic representation of the real robot. For this, we use diagrams similar to the ones presented previously, with non-linearized equations, and we input wind speeds of 2 m/s in the lateral surface of the robot after 10 seconds of simulation. The graphic result is represented in Figure 7.

Observe that the proposed controller is effective even in non-linear systems, although the response becomes more committed. However, a concern was aroused about the wind speed limits of operation which the controller is still effective.

(a)

(b)
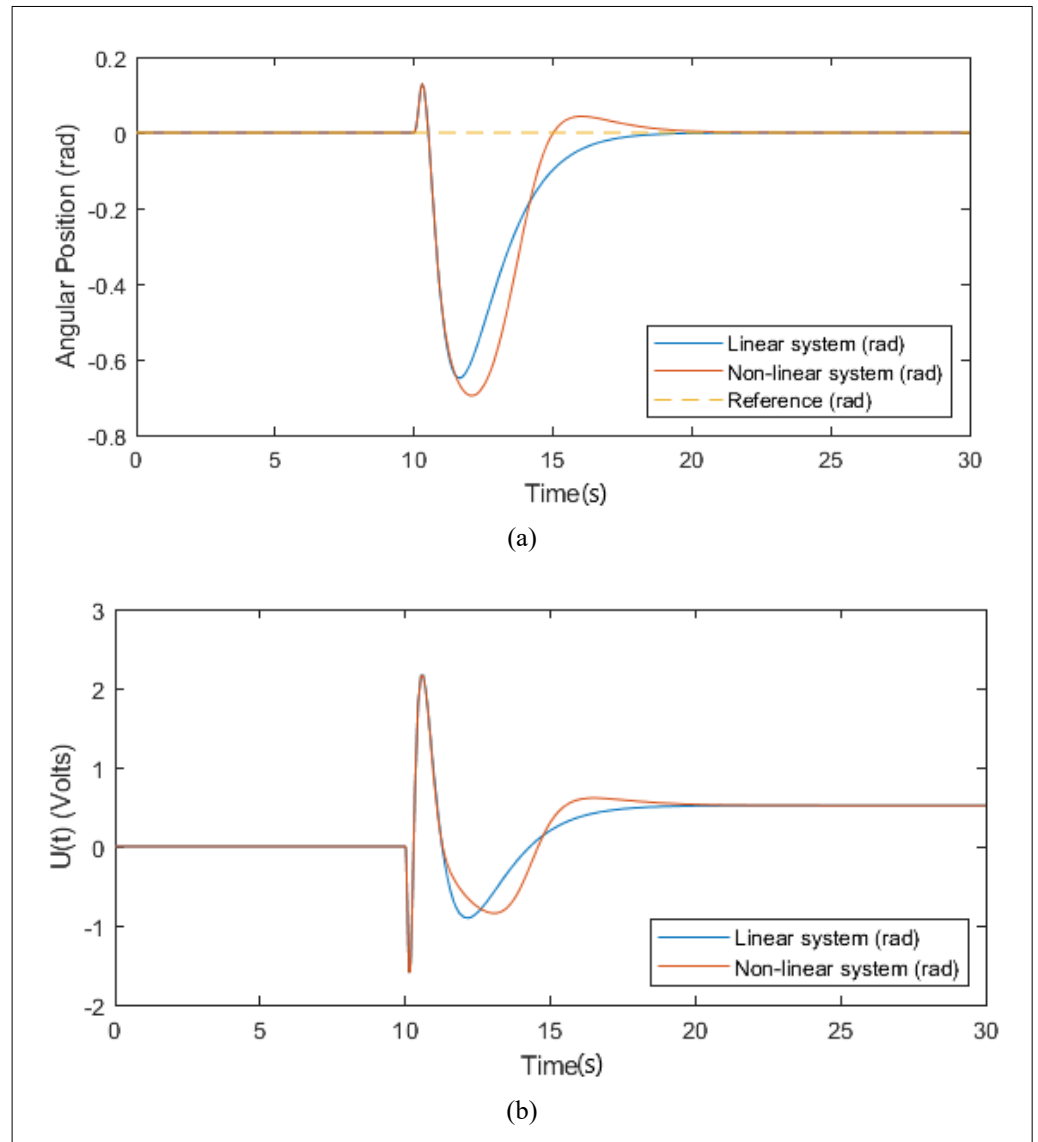
3.1.1 Controller limits (wind speed)

Note that because of the physical limits of the battery voltage, as well as the fact that the controller was designed using a linear model, the robot can fall from the wire at some wind velocities.

Because of this, it is interesting to find the limit of the amplitude of the disturbance (wind speed on the lateral surface of the robot) so that the lateral balance controller can still eliminate the steady-state error.

In this case, we performed tests to find these limits. Using a try-error method, several simulations were done. We conclude that the robot disequilibrium can be fitted in two situations: when there is a high momentary variation in the wind speed (wind gusts), or when there is a gradual increase in the speed, reaching a limit higher than the previous one.

For the first situation, we will denominate the wind gusts as $\Delta q(t)$. To find the limit value of $\Delta q(t)$. that takes the robot to the disequilibrium we performed empirical tests in simulations on Simulink™, changing the value of $\Delta q(t)$. in a step block and looking for the system response in a closed-loop with the proposed controller. With that, we found the value of $\Delta q_{max}(t) \approx 2.4 m/s$, using the parameters of Table 1, as shown in Figure 8.

(a)

(b)

(c)
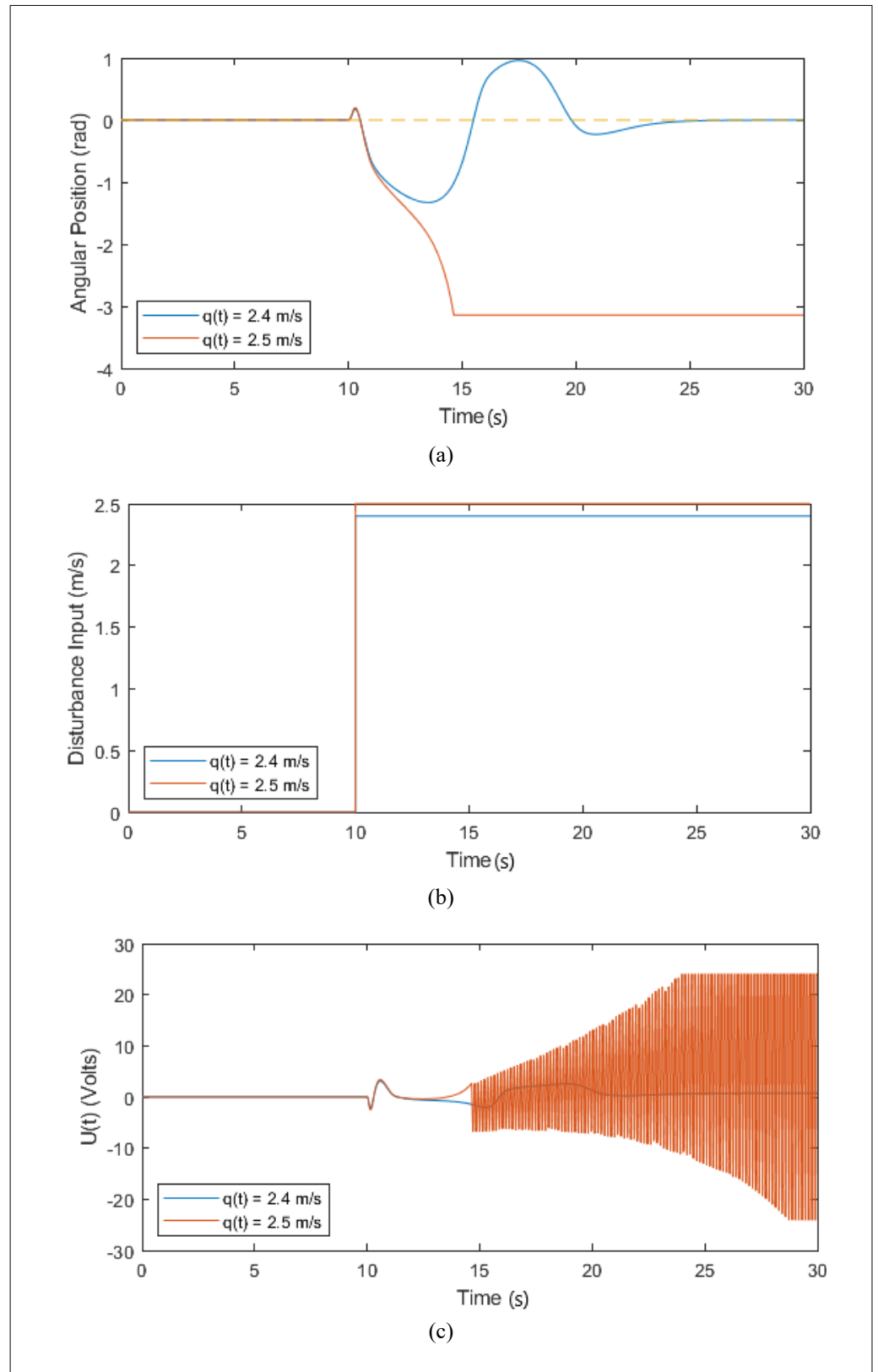
Note that above $\Delta q \approx 2.4$ m/s the robot falls do $\theta = -\pi$ rad (totally fallen) because the control action finds the saturation of 24 V.

Despite finding $\Delta qmax \approx 2.4$ m/s, it is possible to control the robot over wind speed disturbances above this limit, if the velocity has a gradual increase. And performing these
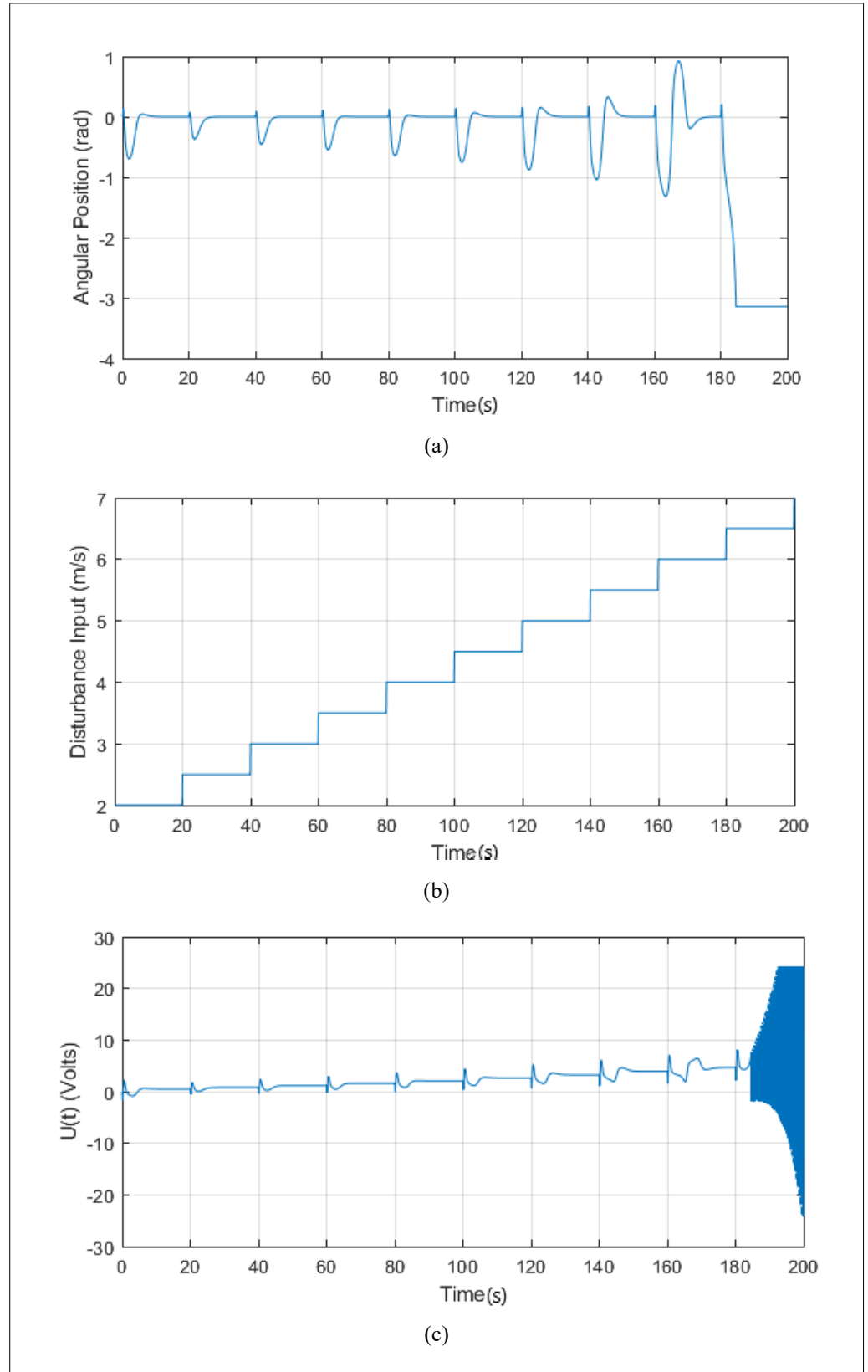
tests with a gradual increase in the wind speed in *q(t) = 0.5 m/s* we can reach a limit between *qmax(t) = 6 m/s* and *qmax(t) = 6.5 m/s*, as shown in Figure 9.

Note that *q(t)* between 6 m/s and 6.5 m/s the robot falls to $\theta = -\pi$ rad (totally fallen) because the control action finds the saturation of 24 V.

(a)

(b)

(c)

3.2 Proposal of a frontal balance controller

With the exposure until here, we can make some conclusions about the lateral balance control of the robot but it is still necessary to elaborate studies on the frontal balance control in this same robot. Given that, the first step for the project of a controller is to model a system in its new axle, and for that, we use the schematic designed in Figure 10.
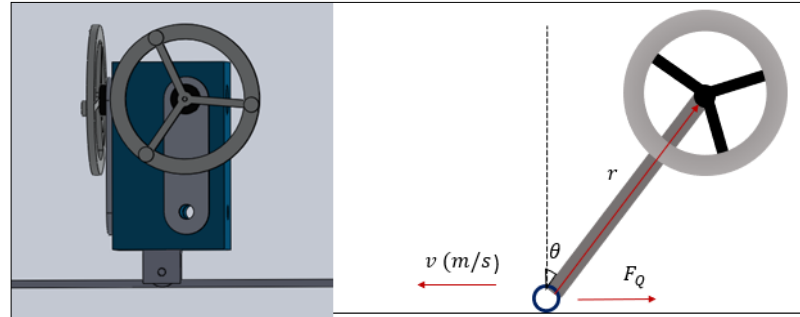
To model this new system, we will rely on the same model obtained for the lateral balance of the robot, changing some parameters and dimensions, and the way the disturbance impacts the system. Dealing with the disturbance, we will consider that the robot runs through the wire according to a speed (m/s), which we will call *q(t)*. Since then, we can describe the impact of *q(t)* in the system as in Equation 21 (Irfan *et al.*, 2018):

$$\tau_q = F_q \times r = m_p \dot{q}(t) r + m_p r^2 \ddot{\theta} \cos(\theta) - m_p r^2 \dot{\theta}^2 \sin(\theta) \tag{21}$$

where m_p is the robot mass and *r* is the height of the robot.

Thus, using Equation 11, changing the torque generated by disturbance, according to Equation (21). With that, we obtain a non-linear model in the following state-space equations (note that these state variables are different than those from the lateral balance controller):

$$\dot{x}_1 = x_2 \tag{22}$$

$$\dot{x}_2 = \frac{Kmgl}{Iso} \sin x_1 - \frac{Bb}{Iso} x_2 + \frac{\left(\dfrac{KtKe}{R} + Br\right)}{Iso} x_3 - \frac{Kt}{RIso} U(t) + \frac{C_a 0{,}613 \, A_e \, r_m}{Iso} q^2(t) \tag{23}$$

$$\dot{x}_3 = \frac{-Kmgl}{Iso} x_1 + \frac{Bb}{Iso} x_2 - \frac{Iso + I_R}{Iso \, I_R}\left(Br + \frac{KeKt}{R}\right) x_3 + \frac{Iso + I_R}{Iso \, I_R}\left(\frac{Kt}{R}\right) U(t) \tag{24}$$
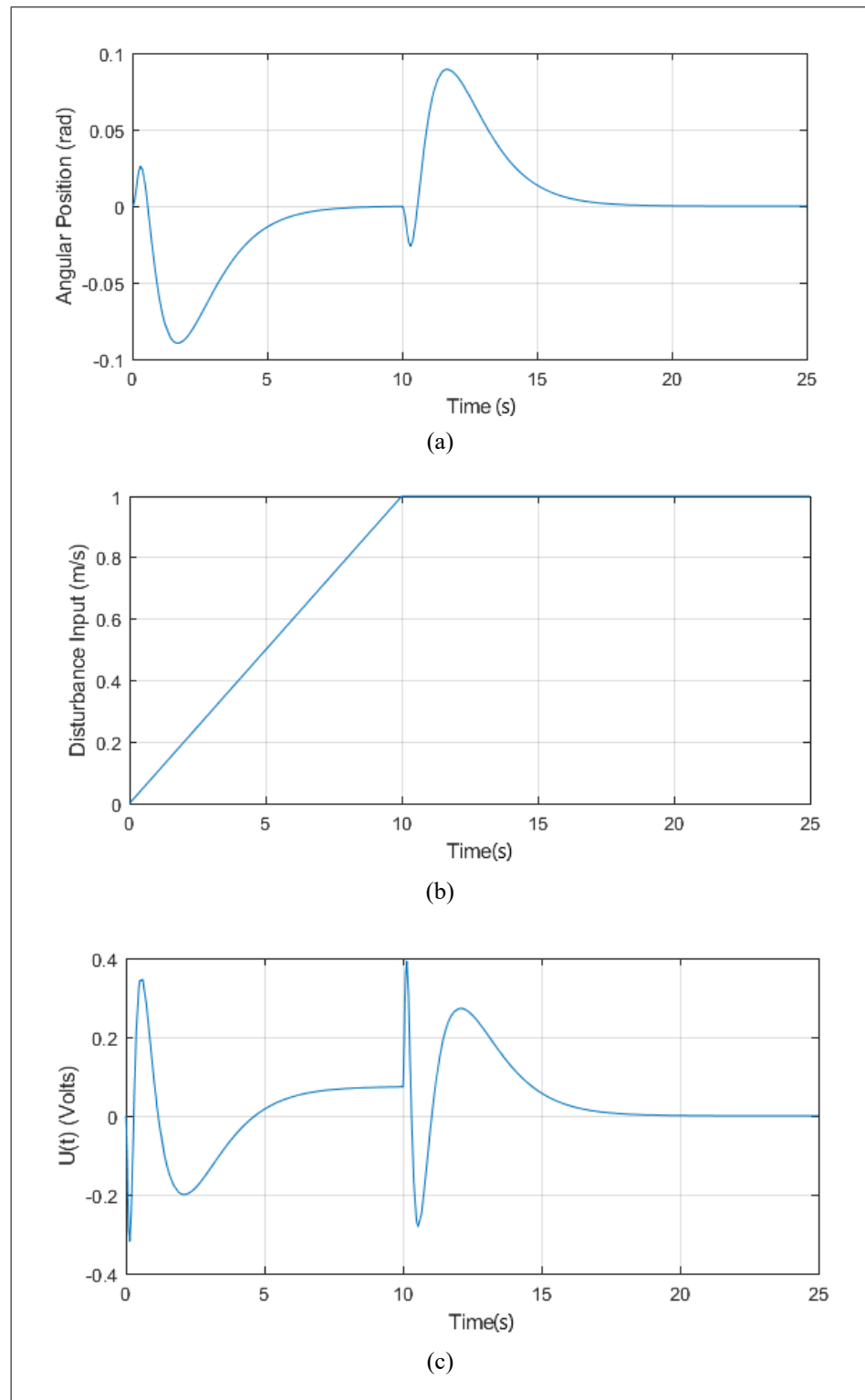
From that, it is possible to project a new state observation feedback controller. The calculus was performed using MATLAB™, and the obtained controller is:

$$C(s) = \frac{110.7 s^3 + 6.5 \times 10^3 s^2 - 6.0 \times 10^3 s + 908.3}{s^3 + 22 s^2 + 2.9 \times 10^3 s} \tag{25}$$

Performing the simulations with the proposed controller, in the non-linear system in Simulink™, over the impact of disturbances *q(t)* (robot accelerating from 0 m/s to 1 m/s) we verify the response, as shown in Figure 11.

(a)

(b)

(c)

From the exposure, it is possible to conclude that the proposed controller is capable of controlling the frontal balance of the robot in the non-linear system for the determined speed and acceleration.

3.2.1 Controller limits (robot speed)

Also, the lateral balance has wind speed limits, and the frontal balance has a limit on the acceleration of the movement through the wire. However, in this case, we can manipulate this disturbance, considering a gradual increase in speed.

After empirical tests, we arrived at the result of maximum acceleration $a_{max} \approx 0.89 \ m/s^2$, as shown by the graphs in Figure 12.

Note that above $q(t) = 0.89 \ m/s^2$ the robot falls to $\theta = \pi$ rad (totally fallen). The graphic of $q(t) = 0.9 \ m/s^2$ is incomplete because of computational limits, caused by the saturation of the controller.

Figure 12 ▶

Simulation results of the tests used to find the limits of robot speed in which the controller is still effective.
a) Angular position.
b) Disturbance signal.
c) Control action.
Source: experimental data

(a)

(b)

(c)
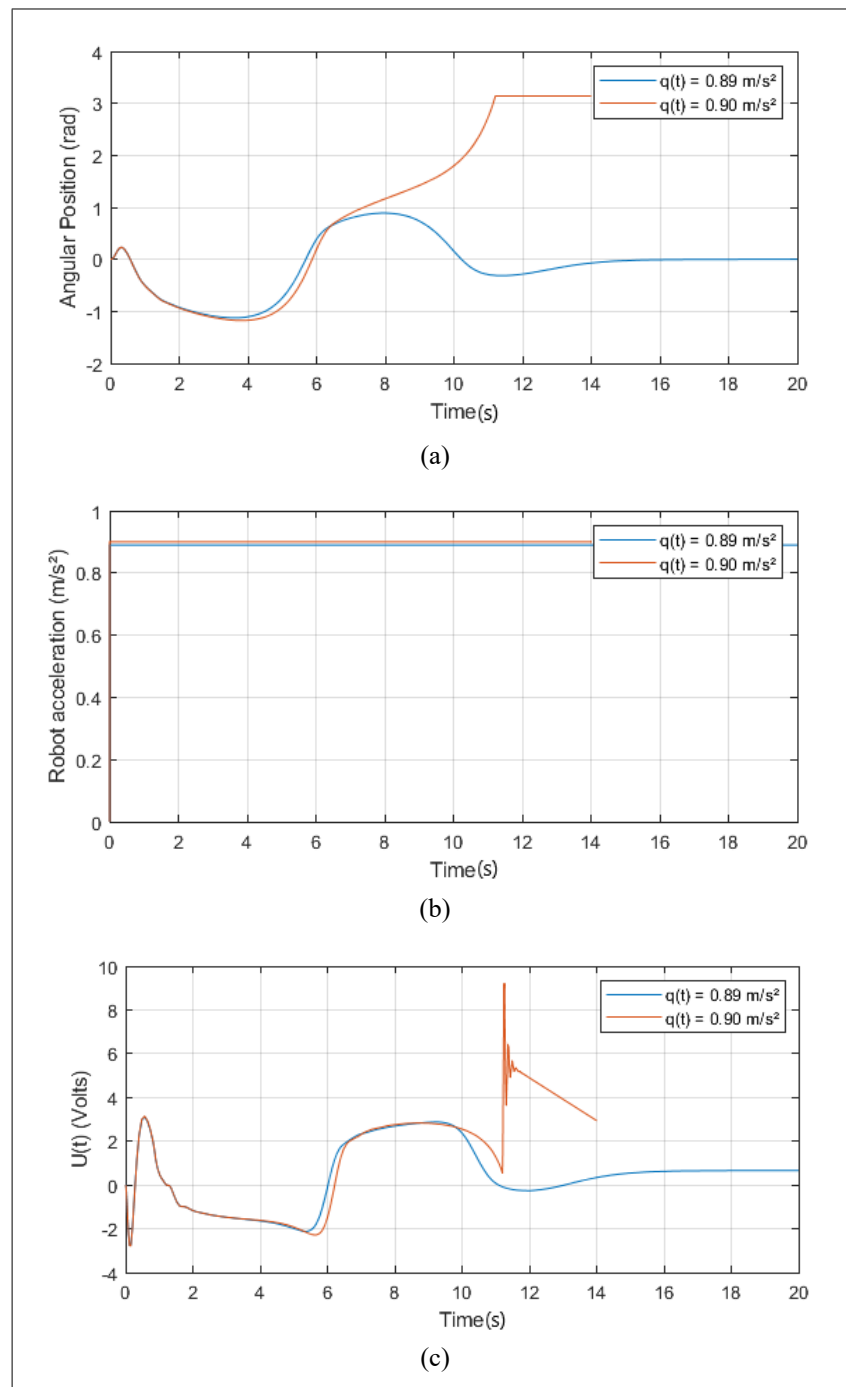
4 Simulation results and discussion

After all, we have a 2D control system, that balances the self-balancing robot in the frontal and lateral axles. These controllers were tested in the non-linear system, with disturbances in its operating limits.

The metrics used to evaluate the effectiveness of the controllers were settling time, integral action error, calculated by Equation 26, integral of the control action, calculated by Equation 27, and maximum disturbance, found in the previous sections.

$$Integral\ Action\ Error\ =\ \int_0^\infty |e(t)|dt \qquad (26)$$

$$Integral\ of\ Control\ Action\ =\ \int_0^\infty |u(t)|dt \qquad (27)$$

The final results and quantitative metrics are described in Table 2.

Metrics	Lateral balance		Frontal balance
Settling time for disturbances	13 s		12 s
Integral action error	6.3583 rad		4.9511 rad
The integral of the control action	18.0662 V		19.0428 V
Maximum disturbance	2.4 m/s (wind gusts)	6.5 m/s (wind speed)	0.89 m/s² (robot acceleration)

By these results, it is possible to compare the use of a controller in standard self-balancing robots, and our robot used for power inspection purposes, without sensing states x_2 and x_3.

Gao, Jin, and Hao (2020) show an artificial intelligence approach for control optimization of a self-balancing robot in lower proportions. Their results were better than ours in settling time: 3 s for lateral balance. Additionally, Ahmed *et al.* (2021) implemented a controller for a simpler system, and using a PID, they have achieved a settling time lower than 2 s.

Finally, Jmel *et al.* (2020) discuss the control performance deterioration when using an observer in the self-balancing robot system. Therefore, it is noted that the settling time, as well as all the other metrics associated, deteriorated without the possibility of sensing all variables.

In addition to these works, our paper shows that the deterioration of the performance control is even greater when looking for power inspection purposes. It is noted that the wind speed is very punitive in the real system, especially since its impact is quadratic as seen in Equation 23. This causes a settling time almost 6 times higher than in systems without disturbance.

Meanwhile, even with all the above, we were able to elaborate a proposed solution for the balance control of a self-balancing robot that works well under some limits of operation, as shown in Table 2. These limits are below the average daily wind velocity in Brazil, according to Raimundo and Santos (2015), validating our work theoretically.

Changing the discussion to the energy inspection context, this solution can be compared with the work of Wang *et al.* (2015), which brings a similar approach to the power transmission line inspection. While their robot has a proposal more robust, our robot brings a simpler construction, with a more limited operating point, as discussed. Also, we can observe that our work is similar to other self-balancing robots as well as in the paper of Sun, Lu, and Yuan (2013), besides presenting the same problems regarding the stabilization time.

5 Conclusion

The studies and analysis done in this paper contribute to the case for the utilization of a self-balancing robot in the inspection of urban wire lines context. However, for a real application and construction of this robot, the authors suggest the utilization of these studies, combined with new research related to possible mechanical approaches to the robot. These approaches must search for the alteration of the center of the mass of the robot to help in the equilibrium, and they can be performed with the addition of a counterweight on the bottom of the robot.

In addition to the mechanical approach, the use of artificial intelligence has been demonstrated very impressively in these contexts. It can be seen, for example, in the papers of Lee and An (2021), that use reinforcement learning methods and neural networks for balance control; Nguyen, Nguyen, and Nguyen (2021) use a neural network combined with a sliding mode controller; Xuan *et al.* (2022) that combine machine learning methods to control a ballbot system with uncertainties.

Now, looking for the application of this self-balancing robot, it is noteworthy that the controller's projects, simulations, and validation tests relied on the theory of books and papers referenced in Section 6. It means that the obtained results with this work do not necessarily represent how the robot would work in real life. Therefore, for future research, it is essential the construct a real robot for tests. After that, is suggested a review of the experiments performed in this paper, with adjustments in parameters and system equations. In this case, research in the area of system identifications for a self-balancing robot, different mechanical designs, and artificial intelligence methods can be the key to the advancement of this scientific technology.

Acknowledgments

Funding

Conflict of interests

The authors declare no conflict of interest.

References

ADABO, G. J. Long range unmanned aircraft system for power line inspection of Brazilian electrical system. **Journal of Energy and Power Engineering**, v. 8, n. 2, p. 394-398, 2014. DOI: http://dx.doi.org/10.17265/1934-8975/2014.02.025.

AHMED, E. Q.; ALJAZAERY, I. A.; AL-ZUBIDI, A. F.; ALRIKABI, H. T. S. Design and implementation control system for a self-balancing robot based on internet of things by using Arduino microcontroller. **Periodicals of Engineering and Natural Sciences**, v. 9, n. 3, p. 409-417, 2021. DOI: http://dx.doi.org/10.21533/pen.v9i3.2178.

ALHASSAN, A. B.; ZHANG, X.; SHEN, H.; XU, H. Power transmission line inspection robots: a review, trends and challenges for future research. **International Journal of Electrical Power & Energy Systems**, v. 118, 105862, 2020. DOI: https://doi.org/10.1016/j.ijepes.2020.105862.

BARBOSA, L.; VELOSO, L. Consumption, domestic life and sustainability in Brazil. **Journal of Cleaner Production**, v. 63, p. 166-172, 2014. DOI: https://doi.org/10.1016/j.jclepro.2013.09.020.

BELASCUEN, G.; AGUILAR, N. Design, modeling and control of a reaction wheel balanced inverted pendulum. *In*: 2018 IEEE BIENNIAL CONGRESS OF ARGENTINA (ARGENCON), 2018, San Miguel de Tucuman. **Proceedings** [...]. San Miguel de Tucuman: IEEE, 2018. p. 1-9. DOI: https://doi.org/10.1109/ARGENCON.2018.8646093.

DOUKAS, H.; KARAKOSTA, C.; FLAMOS, A.; PSARRAS, J. Electric power transmission: An overview of associated burdens. **International Journal of Energy Research**, v. 35, n. 11, p. 979-988, 2011. DOI: https://doi.org/10.1002/er.1745.

DU, L.; ZHAO, Z.; PANG, C.; FANG, Z. Drag force micro solid state silicon plate wind velocity sensor. **Sensors and Actuators A: Physical**, v. 151, n. 1, p. 35-41, 2009. DOI: https://doi.org/10.1016/j.sna.2009.02.003.

GAO, T.; JIN, J.; HAO, X. A single-ball-driven self-balancing robot controller based on genetic algorithm optimization. *In*: INTERNATIONAL CONFERENCE ON ARTIFICIAL INTELLIGENCE AND ADVANCED MANUFACTURE (AIAM2020), 2., 2020, Manchester. **Proceedings** […]. Manchester: ACM, 2020. p. 453-457. DOI: https://dx.doi.org/10.1145/3421766.3421789.

HAN, S.; HAO, R.; LEE, J. Inspection of insulators on high-voltage power transmission lines. **IEEE Transactions on Power Delivery**, v. 24, n. 4, p. 2319-2327, 2009. DOI: https://doi.org/10.1109/TPWRD.2009.2028534.

IRFAN, S.; MEHMOOD, A.; RAZZAQ, M. T.; IQBAL, J. Advanced sliding mode control techniques for inverted pendulum: modelling and simulation. **Engineering**

Science and Technology, an International Journal, v. 21, n. 4, p. 753-759, 2018. DOI: https://doi.org/10.1016/j.jestch.2018.06.010.

JALAL, M. F. A.; SAHARI, K. S. M.; FEI, H. M.; LEONG, J. C. T. Design and development of three arms transmission line inspection robot. **Journal of Robotics, Networking and Artificial Life**, v. 5, n. 3, p. 157-160, 2018. DOI: https://doi.org/10.2991/jrnal.2018.5.3.3.

JMEL, I.; DIMASSI, H.; SAID, S. H.; M'SAHLI, F. Adaptive observer-based output feedback control for two-wheeled self-balancing robot. **Mathematical Problems in Engineering**, v. 2020, 5162172, 2020. DOI: https://doi.org/10.1155/2020/5162172.

KAYGUSUZ, K. Sustainable development of hydroelectric power. **Energy Sources**, v. 24, n. 9, p. 803-815, 2002. DOI: https://doi.org/10.1080/00908310290086725.

LEE, C.; AN, D. Reinforcement learning and neural network-based artificial intelligence control algorithm for self-balancing quadruped robot. **Journal of Mechanical Science and Technology**, v. 35, n. 1, p. 307-322, 2021. DOI: https://doi.org/10.1007/s12206-020-1230-0.

LUQUE-VEGA, L. F.; CASTILLO-TOLEDO, B.; LOUKIANOV, A.; GONZALEZ-JIMENEZ, L. E. Power line inspection via an unmanned aerial system based on the quadrotor helicopter. *In*: IEEE MEDITERRANEAN ELECTROTECHNICAL CONFERENCE (MELECON 2014), 17., 2014, Beirut. **Proceedings** […]. Beirut: IEEE, 2014. p. 393-397. DOI: https://doi.org/10.1109/MELCON.2014.6820566.

NGUYEN, D.-M.; NGUYEN, V.-T.; NGUYEN, T.-T. A neural network combined with sliding mode controller for the two-wheel self-balancing robot. **International Journal of Artificial Intelligence (IAES)**, v. 10, n. 3, p. 592-601, 2021. DOI: http://doi.org/10.11591/ijai.v10.i3.pp592-601.

OGATA, K. **Modern control engineering**. 5th ed. Upper Saddle River, NJ: Prentice Hall, 2010.

OLIVEIRA, N. C. C. A grande aceleração e a construção de barragens hidrelétricas no Brasil. **Varia Historia**, v. 34, n. 65, p. 315-346, 2018. DOI: https://doi.org/10.1590/0104-87752018000200003. In Portuguese.

OLSSON, H.; ÅSTRÖM, K. J.; WIT, C. C.; GÄFVERT, M.; LISCHINSKY, P. Friction models and friction compensation. **European Journal of Control**, v. 4, n. 3, p. 176-195, 1998. DOI: https://doi.org/10.1016/S0947-3580(98)70113-X.

RAIMUNDO, D. R.; SANTOS, I. F. S. Estudo de um projeto para geração de energia eólica no Brasil: viabilidade econômica e emissões evitadas. **Revista Brasileira de Energias Renováveis**, v. 4, n. 4, p. 65-75, 2015. DOI: http://dx.doi.org/10.5380/rber.v4i4.44156. In Portuguese.

ROUSSIALIAN, M.; AL-ZANBARAKJI, H.; KHAWAND, A.; RAHAL, A.; OWAYJAN, M. Design and development of a pipeline inspection robot. *In*: RIZK, R.; AWAD, M. (ed.). **Mechanism, machine, robotics, and mechatronics sciences**. Cham: Springer, 2019. p. 43-52. DOI: https://doi.org/10.1007/978-3-319-89911-4_4.

SANTOS, M. **A urbanização brasileira**. 1st ed. São Paulo: EdUSP, 2013. In Portuguese.

SHAIKAT, A. S.; HUSSEIN, M. R.; TASNIM, R. Design and development of a pipeline inspection robot for visual inspection and fault detection. *In*: PAN, I.; MUKHERJEE, A.; PIURI, V. (ed.). **Proceedings of Research and Applications in Artificial Intelligence**. Singapore: Springer, 2021. p. 243-253. DOI: https://doi.org/10.1007/978-981-16-1543-6_23.

SUN, C.; LU, T.; YUAN, K. Balance control of two-wheeled self-balancing robot based on linear quadratic regulator and neural network. *In*: INTERNATIONAL CONFERENCE ON INTELLIGENT CONTROL AND INFORMATION PROCESSING (ICICIP), 4., 2013, Beijing. **Proceedings** […]. Beijing: IEEE, 2013. p. 862-867. DOI: https://doi.org/10.1109/ICICIP.2013.6568193.

TRANSMOTEC. **DC-motors 12VDC 6A 8400rpm 53W**. Product-name: 770-7040-CC: Datasheet. 2021. Available at: https://www.transmotec.com/product/770-7040-cc/. Accessed on: 14 jun. 2022.

WANG, W.; HE, T.; WANG, H.; CHEN, W. Balance control of a novel power transmission line inspection robot. *In*: 2015 IEEE INTERNATIONAL CONFERENCE ON ROBOTICS AND BIOMIMETICS (ROBIO), 2015, Zhuhai. **Proceedings** […]. Zhuhai: IEEE, 2015. p. 1882-1887. DOI: https://doi.org/10.1109/ROBIO.2015.7419047.

XIE, X.; LIU, Z.; XU, C.; ZHANG, Y. A multiple sensors platform method for power line inspection based on a large unmanned helicopter. **Sensors**, v. 17, n. 6, 1222, 2017. DOI: https://doi.org/10.3390/s17061222.

XUAN, H. L.; HOANG, Q.-D.; LEE, S.-G.; XUAN, D. P.; VIET, H. T.; VAN, M. P.; VAN, H. P.; VIET, H. P.; TUAN, P. D.; NGUYEN, D. A. Adaptive hierarchical sliding mode control using an artificial neural network for a ballbot system with uncertainties. **Journal of Mechanical Science and Technology**, v. 36, n. 2, p. 947-958, 2022. DOI: https://doi.org/10.1007/s12206-022-0141-7.

ZHANG, H. Y.; ZHU, S. L.; ZHANG, Y.; LOU, Q.; ZHANG, L. Research and implementation of condition-based maintenance technology system for power transmission and distribution equipments. **Power System Technology**, v. 33, n. 13, p. 70-73, 2009.